J Solid State Electrochem (2011) 15:2213–2219
DOI 10.1007/s10008-010-1224-4

ORIGINAL PAPER

Microstructure and infrared reflectance modulation properties in DC-sputtered tungsten oxide films

Jun Zhang · Xiu-li Wang · Yuan Lu · Ya Qiao · Xin-hui Xia · Jiang-ping Tu

Received: 15 September 2010 / Revised: 17 October 2010 / Accepted: 19 October 2010 / Published online: 24 November 2010
© Springer-Verlag 2010

Abstract Tungsten oxide (WO_3) films were deposited on indium tin oxide glass by reactive DC magnetron sputtering of a tungsten target in an oxygen and argon atmosphere at different substrate temperatures. Infrared reflectance modulation properties of the films were investigated in the wavelength range of 2.5–25 μm. The morphology and structure of the films are strongly dependent on the substrate temperature, and therefore have a great influence on infrared reflectance modulation properties. The charge capacity and diffusion coefficient of H^+ ions in WO_3 films decrease, and the infrared reflectance modulation and color efficiency first increase and then decrease with increasing the deposition temperature. The values achieve a maximum of 40% and 18.5 $cm^2\ C^{-1}$, respectively, at 9 μm and 250 °C.

Keywords Tungsten oxide · Thin film · Electrochromism · Infrared reflectance modulation

Introduction

Electrochromism refers to the persistent and reversible change of optical properties by an applied voltage pulse. It was first discovered by S.K. Deb [1] in tungsten oxide in 1969. The potential applications of electrochromic materials include many technological areas, such as smart windows [2–6], antiglare automotive mirrors [7], full-angle information displays [8], etc. Most of the applications have been based on the optical changes in the visible spectrum [9–13]. Furthermore, electrochromic materials can be also used in infrared (IR) region, such as thermal control of satellites [14] and infrared camouflage [15]. Although many noteworthy works [14–23] have been done in the last decade, studies on IR region of electrochromic materials are far from sufficient. There are two windows of 3–5 μm and 8–14 μm in the atmosphere in which infrared ray can pass through. Out of the windows, the infrared ray would be absorbed by air. Furthermore, the 8–14-μm window is also known as the thermal wavelength. Therefore, researches were focused on the infrared modulation properties in these two windows.

Tungesten oxide (WO_3) film is most extensively studied among various electrochromic materials. The film changes from light yellow or bleach to dark blue under applied voltage, meanwhile the infrared properties change as well. Elctrochromism in WO_3 is due to the formation of H_xWO_3 by double injection of electron and ion when a negative voltage is applied. This process is reversible:

$$WO_3\,(\text{transparent}) + xH^+ + xe^- \rightleftarrows H_xWO_3\,(\text{blue}) \quad (1)$$

The electrochromic properties of WO_3 are dependent on many factors, such as crystallinity, crystal form, stoichiometry, surface morphology, and so on. The crystallinity is a

J. Zhang · X.-l. Wang (✉) · X.-h. Xia · J.-p. Tu (✉)
State Key Laboratory of Silicon Materials and Department of Materials Science and Engineering, Zhejiang University, Hangzhou 310027, China
e-mail: wangxl@zju.edu.cn

J.-p. Tu
e-mail: tujp@zju.edu.cn

Y. Lu · Y. Qiao
Key Laboratory of Infrared and Low Temperature Plasma of Anhui Province, Hefei Electronic Engineering Institute, Hefei 230037, China

very important factor determining the electrochemical properties, e.g., the response time and charge insertion, and optical properties, e.g., the range of modulation in different wave bands.

The dependence of electrochromic properties on the crystallinity of WO_3 film in the visible region has been investigated in detail by many researchers [24–27], but it remains rare in the infrared region [18]. In this present work, the effects of deposition temperature (substrate temperature T_s) on the electrochemical and infrared reflectance modulation properties of WO_3 films were investigated.

Experimental

WO_3 films were deposited on indium tin oxide (ITO) glass (sheet resistance, 25 ohms/square; average IR reflectance, 95.6%) and Si <100> substrates by reactive DC magnetron sputtering of a metallic tungsten target (purity 99.9%). The sputter chamber was initially evacuated to a base pressure of 5.0×10^{-3} Pa. Pure oxygen and argon gas were introduced into the chamber with the mass flow ratio of 1: 4, and the deposition pressure was kept at 0.45 Pa. The target–substrate distance was set at 8 cm. The substrates were heated by radiant exposure, and the temperature range was from room temperature (RT) to 300 °C. Due to the heating effect of the plasma, the substrate temperature was about 50 °C (we regarded it as RT) without being heated by radiant exposure. The sputtering power was 84 W, and films with a thickness of ca. 350 nm were obtained with a deposition rate of 0.23 $\mathrm{nm s^{-1}}$. After deposition, the substrates were gradually cooled to room temperature at a cooling rate of 3 $\mathrm{°C s^{-1}}$ in the vacuum chamber and then taken out for further characterization.

The surface morphology was characterized by a field emission scanning electron microscopy (FESEM, Hitachi S-4800) equipped with an EDX attachment (HORIBA EMAX400) and the film thickness was determined by cross-sectional SEM. The structure of the films was examined by means of X-ray diffraction [XRD, PANalytical X'Pert PRO diffractometer, CuKα radiation (λ= 1.54056 Å)]. The 2θ ranged from 20° to 80° with a step of 0.02° and a scanning speed of $2.4°\mathrm{min}^{-1}$. The transmittance spectra of the as-deposited films were recorded in the wavelength range of 400 nm to 1,000 nm with the Spectrophotometer-721 (Shanghai Jinghua Tech. Instruments Co., Ltd.). Raman spectra were obtained with a LabRam HR system (Jobin-Yvon, France) using a 20-mW Ar (514 nm) laser. Measurements were conducted in backscattering mode with a spectrum resolution of 1 cm^{-1}.

The electrochemical measurements were carried out in a three-electrode cell filled with 0.1 M H_2SO_4 electrolyte at room temperature (25 °C). A platinum foil 2×2 cm in size served as the counter electrode and an Ag/AgCl electrode was the reference electrode. The configuration of the cell was as follows:

$$\mathrm{ITO/WO_3 film/0.1\,M\,H_2SO_4/Pt;\,Ag/AgCl}$$

The experiments were performed on a CHI660C electrochemical workshop. Voltages between −1.0 V and +1.0 V relative to the Ag/AgCl electrode were applied at a scan rate of 50 $\mathrm{mV s^{-1}}$.

The IR reflectance spectra of the films (as-deposited, colored, and bleached states) were measured using an IR spectrophotometer NICOTCT at 15° angle of incidence in the wavelength range from 2.5 to 25 µm. A gold mirror was used as a reflectance reference (R≈99% in IR region).

Results and discussion

Figure 1 shows the XRD patterns of the WO_3 films deposited on silicon (100) wafer substrates at temperatures of RT to 300 °C. The film deposited at RT shows no significant peaks, indicating that it is amorphous. The films deposited at T_s=100 °C, 200 °C, 250 °C, and 300 °C can be indexed as monoclinic WO_3 phase (JCPDS file 71–2141) and those reported by others [28,29]. The crystallinity of the WO_3 films increased obviously with the substrate temperature.

The surface topographies of WO_3 films deposited at different substrate temperatures were observed by SEM. As shown in Fig. 2, in general all the films appear homogeneous and smooth. At the higher temperatures, the films appear to have more boundaries, which indicate that the films tend to have an island growth mechanism. EDX results showed that the O/W ratios were 2.98±0.05, 3.00± 0.05, 3.02±0.05, 3.05±0.05, and 3.03±0.05, for the films deposited at T_s=50 °C, 100 °C, 200 °C, 250 °C, and 300 °C, respectively.

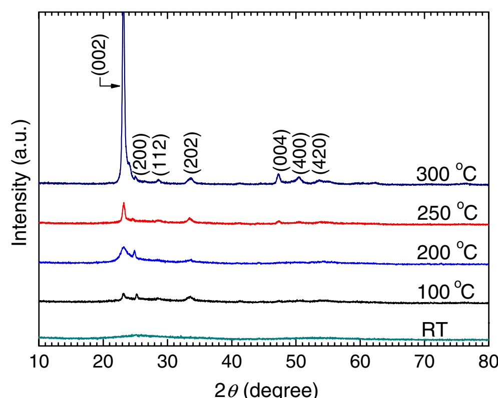

Fig. 1 XRD patterns of WO_3 films deposited at temperatures between RT and 300 °C

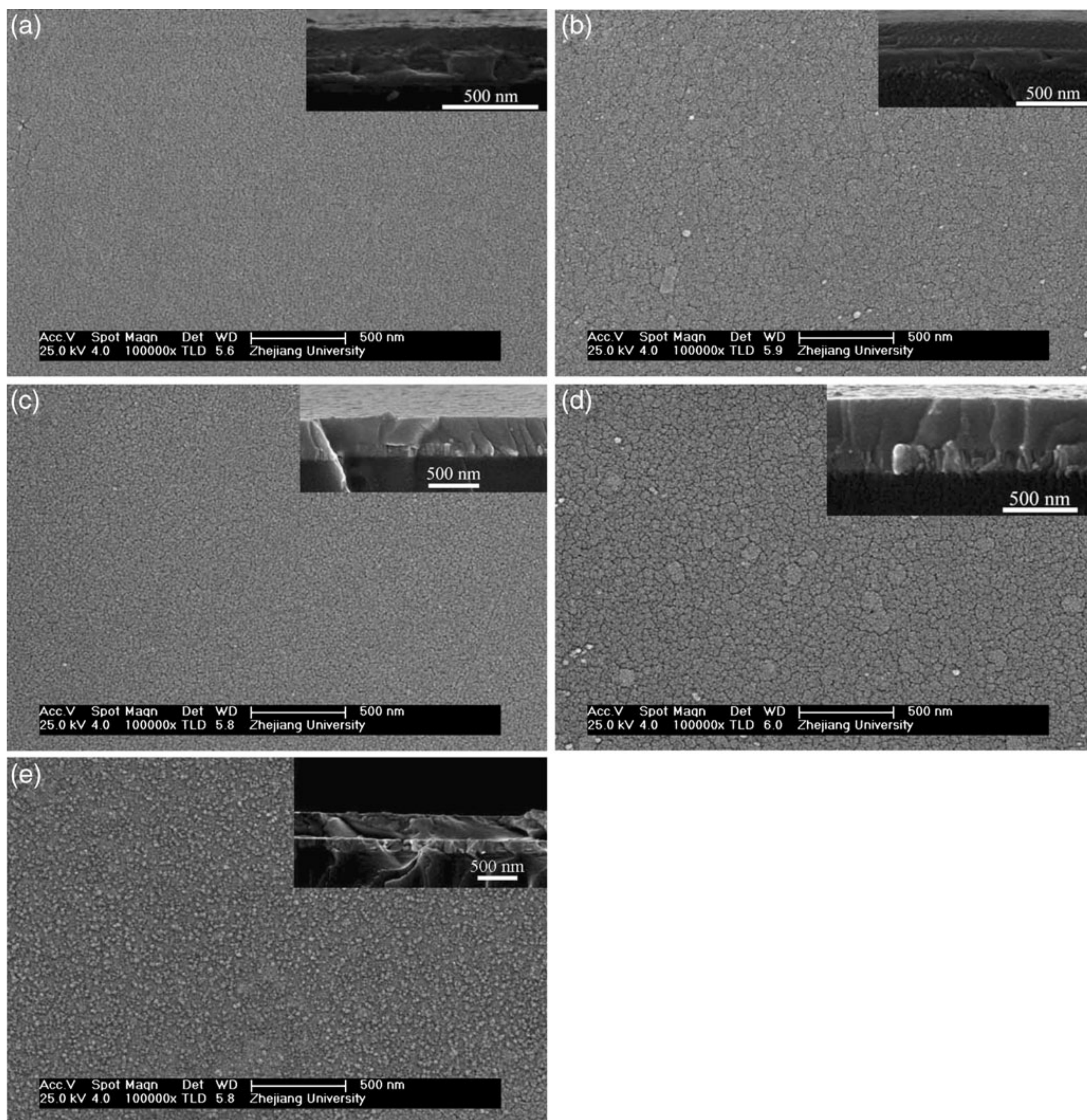

Fig. 2 SEM micrographs of WO_3 films. **a** Room temperature, **b** 100 °C, **c** 200 °C, **d** 250 °C, and **e** 300 °C (*insets* are cross-sectional views)

The transmittance spectra of the as-deposited films on ITO glass substrate were recorded in the wavelength range of 400 nm to 1,000 nm. As shown in Fig. 3, all the films show quite high transmittance (~80%) in the visible range from 400 to 700 nm and similar interference fringe patterns, indicating that the stoichiometry as well as the film thickness has no significant variation in the range of deposition temperature.

IR reflectance of colored and bleached WO_3 films deposited on ITO glass in the wavelength range of 2.5–25 μm are shown in Fig. 4. The absorption features around 6 μm (~1,600 cm^{-1}) and 3 μm (~3,400 cm^{-1}) are caused by H–O–H deformation and O–H stretching vibrations, respectively [9,30]. This phenomenon indicates that water was adsorbed in the films during the deposition process or outside of the vacuum chamber [31]. A broad absorption

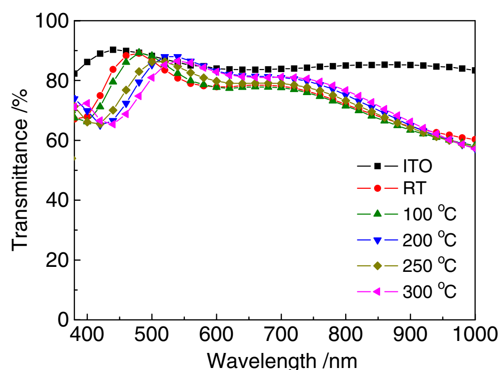

Fig. 3 VIS-NIR transmittance of WO_3 films deposited on ITO glass substrates

is found around 16–17 μm (between 600 and 800 cm^{-1}). This is characteristic for a disordered W–O–W framework [9,28,30]. This absorption became very weak for the film deposited at T_s=300 °C, indicating that a well crystalline WO_3 film was obtained. A weak absorption at ~8 μm is attributed to the ITO substrate [32]. The peak near 10 μm, i.e., ~970 cm^{-1}, is contributed from asymmetric stretching vibrations of W=O bonds mainly on internal surfaces [7,28,33]. The colored state of crystalline WO_3 films (Fig. 4c, d, e) do not show significant peaks, suggesting that the films are non-transparent in the IR region, that is to say the IR light cannot arrive to the ITO surface, but can be reflected by the surface of the films.

The film deposited at room temperature shows IR reflectance modulation in the order of 10% in the wavelength range of 8–22 μm. For the films with a thickness of 350 nm in this present work, IR modulation properties are improved remarkably by heating the substrates during the deposition process. Figure 5 shows the average modulation range Δ*R* of the films deposited at different temperatures in the wavelength range of 8–14 μm (the atmosphere window). The average Δ*R* value reaches up to 35% for the film deposited at 250 °C and then decreases sharply for the film deposited at 300 °C. IR emissivity (ε) in wavelength range from λ_1 to λ_2 can be calculated from the reflectance spectra using the following equation:

$$\varepsilon = \frac{\int_{\lambda_2}^{\lambda_1} [1 - R(\lambda)] M_b(\lambda, T) d\lambda}{\int_{\lambda_2}^{\lambda_1} M_b(\lambda, T) d\lambda} \qquad (2)$$

where $R(\lambda)$ is the measured reflectance and $M_b(\lambda,T)$ is the blackbody spectral emittance. In this calculation the temperature was fixed at 300 K, and λ_1 and λ_2 were 8 and 14 μm, respectively. Thus, the largest IR emissivity modulation of 0.27–0.5 in 8–14 μm is obtained at T_s= 250 °C. This result is comparable to the emittance of the device with a 160-nm thick crystalline WO_3 as the modulation layer [15], but less than that of the WO_3/Ta_2O_5/NiO devices [14]. It has been reported that a 1.45-μm thick amorphous WO_3 film exhibit an emittance modulation range of 0.52–0.72 with intercalation of Li^+ [34]. This disagreement should be owing to the film thickness. It has been confirmed that a thicker amorphous WO_3 showed better emittance modulation properties [35].

In order to investigate the microstructure of films deposited at different substrate temperatures and the changes of microstructure during the intercalation and deintercalation of H^+, Raman shift spectra, which can provide more information in details than IR spectra, were used. As shown in Fig. 6, all the spectra of the films exhibit two regions: (1) 650–850 cm^{-1} corresponding to the stretching vibrations of O–W^{6+}–O bonds; (2) 250–350 cm^{-1} corresponding to the bending vibrations of O–W–O bonds [36]. Raman shift observed below 200 cm^{-1} corresponds to the lattice modes. The band around 951 cm^{-1} is assigned to the stretching mode of the short terminal W=O bond, which is because of the adsorbed water molecules on films. It has been reported that the electrochromic properties would be enhanced by the presence of water [2]. In this work, the water content first increases with the substrate temperature and then decreases, hence the electrochromic properties have the same tendency. The presence of well-resolved and sharp Raman bands for the stretching and bending vibration regions and the reduction in intensity for W=O stretching mode suggest the enhancement of crystallization of the film deposited at T_s=300 °C. It is in agreement with the XRD results. The FWHM (full wave at half maximum) of the Raman band around 807 cm^{-1} reflects the structural order in terms of bond length and angle of the O–W–O bonding [37]. The Raman band for the films becomes sharper with increasing the substrate temperature, implying the increase of structural order. For the films deposited at 250 °C and 300 °C, when H^+ is intercalated into them, the Raman band at 692 cm^{-1} becomes indefinite (Fig. 6b), indicating a disordered O–W–O framework due to H^+ intercalation.

Figure 7 shows the cyclic voltammograms of WO_3 films deposited at different substrate temperatures. The apparent color turned from transparent to blue and infrared reflectance properties are also changed as the voltage scanned from +1.0 V to −1.0 V. This process is associated with intercalation and deintercalation of H^+ ions and electrons in the films (reaction 1).

The characteristic parameters for the cyclic voltammograms of WO_3 thin films deposited at different temperatures are listed in Table 1. The diffusion coefficient of H^+

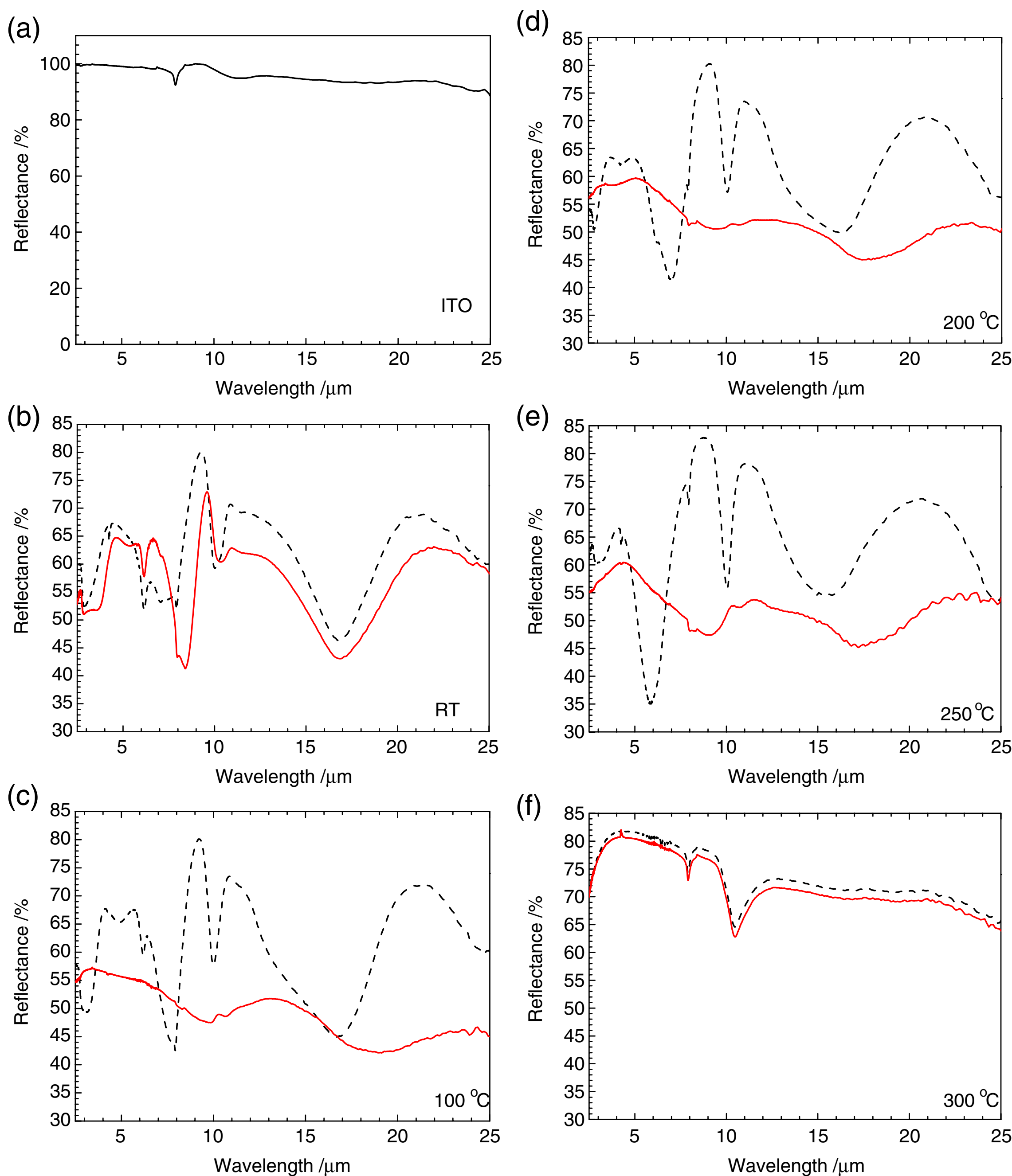

Fig. 4 IR reflectance in the wavelength range of 2.5–25 μm. **a** Bare ITO substrate, and films deposited at **b** room temperature, **c** 100 °C, **d** 200 °C, **e** 250 °C, and **f** 300 °C, *solid curves*, colored state; *dashed curves*, bleached state

intercalation and deintercalation is calculated from the Randles-Sevcik equation [38]:

$$i_p = 2.687 \times 10^5 n^{3/2} v^{1/2} D^{1/2} C \quad (3)$$

where n is the number of electrons and assumed to be 1, v is the rate at which the potential is swept (volts per second), D is the diffusion coefficient (square centimeter per second), C is the concentration of active ions in the solution (mole per cube centimeter), and i_p is the peak current density [anodic peak current i_{pa} (milliampere per square centimeter)]. The results are also listed in Table 1. The diffusion coefficient of the films decreases with the increase of deposition temperature. Obviously, the decrease of diffusion coefficient is due to the improved crystalline integrity. H^+ ions diffuse in loose amorphous WO_3 films more easily than in dense crystalline WO_3 films.

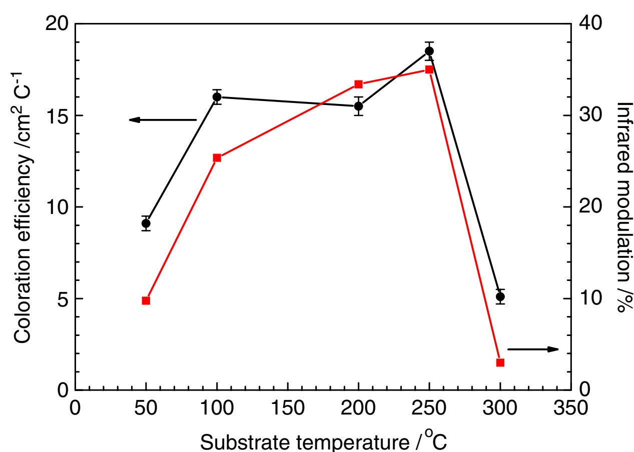

Fig. 5 Average ΔR of films deposited at different temperatures in the wavelength range of 8–12 μm and the CE value of films deposited at different temperatures at 9 μm

In order to evaluate the electrochromic property of films, coloration efficiencies are calculated. We define coloration efficiency (CE) as:

$$\mathrm{CE} = \Delta OD/\Delta Q \quad (4)$$

$$\Delta OD = \log(R_b/R_c) \quad (5)$$

where R_b and R_c refer to reflectance of films in bleached and colored states, respectively. A higher value of CE indicates that the film exhibits larger infrared modulation with less intercalation and deintercalation of H^+ ions and electrons into the films. The CE values at 9 μm obtained from cyclic voltammograms and infrared reflectance are also shown in Fig. 5. The color efficiency first increases and then decreases with the deposition temperature. The maximum value of 18.5 cm^2C^{-1} is achieved at 250 °C.

Conclusions

WO_3 films were deposited by reactive DC magnetron sputtering at different substrate temperatures. With the increase of the deposition temperature, the diffusion coefficient of H^+ ions in the WO_3 films decrease. The infrared reflectance modulation and color efficiency (CE) first increase and then decrease with the deposition temperature, and maximum values of 40% and 18.5 cm^2C^{-1}, respectively, are achieved at 250 °C and 9 μm. The WO_3 films with reflectance modulation (higher than 30%) in infrared band can be fabricated into devices, which have considerable applications in thermal control and infrared camouflage.

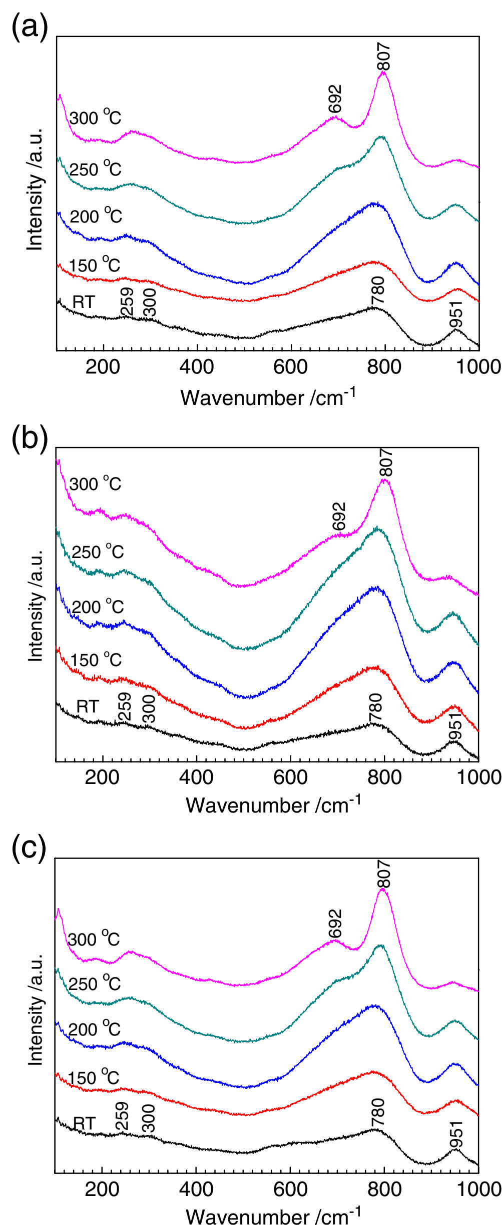

Fig. 6 Raman shift spectra of **a** as-deposited films, **b** films intercalated of H^+, **c** films deintercalated of H^+

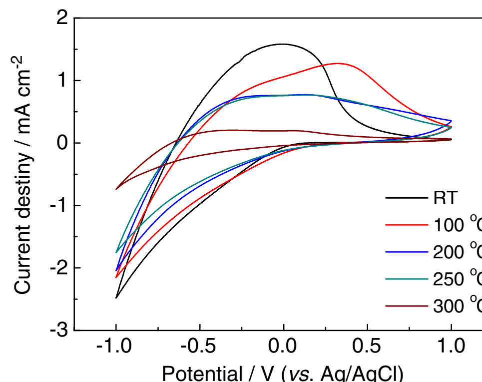

Fig. 7 The cyclic voltammograms for WO_3 films deposited at **a** room temperature, **b** 100 °C, **c** 200 °C, **d** 250 °C, and **e** 300 °C at a scan rate of 50 mVs^{-1}

Acknowledgement This work was supported by Zhejiang University K.P. Chao's High Technology Development Foundation (grant no. 2008ZD001).

Table 1 The characteristic parameters for the cyclic voltammograms of WO_3 thin films deposited at different temperatures

T_s	Q_a (mC cm^{-2})	Q_c (mC cm^{-2})	i_{pa} (mA cm^{-2})	D_{pa} (10^{-11} cm s^{-1})
RT	34.5±0.1	−41.2±0.1	1.58	6.96
100 °C	34.7±0.1	−37.9±0.1	1.27	4.50
200 °C	25.7±0.1	−30.8±0.1	0.774	1.67
250 °C	25.2±0.1	−27.9±0.1	0.767	1.64
300 °C	4.7±0.1	−10.2±0.1	0.204	0.012

T_s substrate temperature; Q_a and Q_c charge capacity of films during cathodic and anodic reactions, respectively; i_{pa} anodic peak current; D_{pa} diffusion coefficient for i_{pa}

References

1. Deb SK (1969) Appl Opt Suppl 3:192–195
2. Deb SK (2008) Sol Energy Mater Sol Cells 92:245–258
3. Zhang J, Tu JP, Xia XH, Qiao Y, Lu Y (2009) Sol Energy Mater Sol Cells 93:1840–1845
4. Zhang J, Wang XL, Xia XH, Gu CD, Zhao ZJ, Tu JP (2010) Electrochim Acta 55:6953–6958
5. Xia XH, Tu JP, Zhang J, Xiang JY, Wang XL, Zhao XB (2010) ACS Appl Mater Interfaces 2:186–192
6. Patil PS (2001) J Solid State Electrochem 6:284–287
7. Lampert CM (2004) Mater Today 7:28–35
8. Moller MT, Asaftei S, Corr D, Ryan M, Walder L (2004) Adv Mater 16:1558–1562
9. Granqvist CG (1995) Handbook of inorganic electrochromic materials. Elsevier, Amsterdam
10. Granqvist CG (2008) Sol Energy Mater Sol Cells 92:203–208
11. Xia XH, Tu JP, Zhang J, Wang XL, Zhang WK, Huang H (2008) Nanotechnology 19:465701
12. Bueno PR, Gabrielli C, Perrot H (2008) Electrochim Acta 53:5533–5539
13. Lusis A, Kleperis J, Pentjuss E (2002) J Solid State Electrochem 7:106–112
14. Hale JS, Woollam JA (1999) Thin Solid Films 339:174–180
15. Franke EB, Trimble CL, Schubert M, Woollam JA, Hale JS (2000) Appl Phys Lett 77:930–932
16. Acosta M, Gonzalez D, Riech I (2009) Thin Solid Films 517:5442–5445
17. Sato R, Kawamura N, Tokumaru H (2008) Appl Surf Sci 254:7676–7678
18. Hutchins MG, Butt NS, Topping AJ, Gallego J, Milne P, Jeffrey D, Brotherston I (2001) Electrochim Acta 46:1983–1988
19. Lin SH, Chen FR, Kai JJ (2008) Appl Surf Sci 254:3357–3363
20. Xia XH, Tu JP, Zhang J, Huang XH, Wang XL, Zhao XB (2010) Sol Energy Mater Sol Cells 94:386–389
21. Bergeron BV, White KC, Boehme JL, Gelb AH, Joshi PB (2008) J Phys Chem C 112:832–838
22. Sauvet K, Rougier A, Sauques L (2008) Sol Energy Mater Sol Cells 92:209–215
23. Deepa M, Srivastava AK, Sharma SN, Govind, Shivaprasad SM (2008) Appl Surf Sci 254:2342–2352
24. Ozkan E, Lee SH, Tracy CE, Pitts JR, Deb SK (2003) Sol Energy Mater Sol Cells 79:439–448
25. Liao CC, Chen FR, Kai JJ (2007) Sol Energy Mater Sol Cells 91:1258–1266
26. Hechavarria L, Hu H, Miranda M, Nicho ME (2009) J Solid State Electrochem 13:687–695
27. Bathe SR, Patil PS (2008) Solid State Ionics 179:314–323
28. Deepa M, Kar M, Agnihotry SA (2004) Thin Solid Films 468:32–42
29. Zayim EO, Liu P, Lee SH, Tracy CE, Turner JA, Pitts JR, Deb SK (2003) Solid State Ionics 165:65–72
30. Guéry C, Choquet C, Dujeancourt F, Tarascon JM, Lassègues JC (1997) J Solid State Electrochem 1:199–207
31. Leftheriotis G, Papaefthimiou S, Yianoulis P (2004) Sol Energy Mater Sol Cells 83:115–124
32. Lee DH, Vuong KD, Condrate RA Sr, Wang XW (1996) Mater Lett 28:179–182
33. Shigesato Y, Hayashi Y, Masui A, Haranou T (1991) Jpn J Appl Phys 30:814–819
34. Larsson AL, Solis J, Niklasson GA (2007) Sol Energy Mater Sol Cells 91:1248–1252
35. Larsson AL, Niklasson GA (2004) Mater Lett 58:2517–2520
36. Lethy KJ, Panda S, Beena D, Vinodkumar R, Sathe V, Pillai VPM (2009) J Phys D Appl Phys 42:185407
37. Shigesato Y (1991) J Appl Phys 30:1457–1462
38. Leftheriotis G, Papaefthimiou S, Yianoulis P (2007) Solid State Ionics 178:259–263